COBEM 2023 27TH INTERNATIONAL CONGRESS OF MECHANICAL ENGINEERING

ABCM Brazilian Society of Mechanical Sciences and Engineering
27th ABCM International Congress of Mechanical Engineering
December 04-08, 2023, Florianópolis-SC, Brazil

COB-2023-1084
NUMERICAL VIBRATION ANALYSIS OF HUMAN MIDDLE EAR IMPLANTED WITH A VIBRATION SENSOR AND A FLAT FLEXIBLE CABLE FOR ELECTRICAL CONNECTION

Vinicius de Moura Paegle
Stephan Paul
Acoustic and Vibration Laboratory, Federal University of Santa Catarina, Florianópolis, 88040-900, Brazil
paeglevini@gmail.com,stephan.paul@ufsc.br

Abstract. *Totally implantable cochlear implants would solve several problems nowadays related to the external sound capturing and processing unit of traditional cochlear implants, but require implantable solutions for sound pick-up and signal processing. The present work aims to analyze by computational models the effect of a flexible cable, proposed to connect the vibration sensor on the ossicular chain to the cochlear implant processor. Numerical models of three different implantable cables were constructed. The most appropriate model of such a cable was then coupled to a FE model of the human middle ear to analyze the behavior of the middle ear when both sensor and cable were attached. The analysis showed that the proposed cable increased the middle ear's stiffness and raised its two first natural frequencies by around 7% and 11% respectively. Also, it was found that the magnitudes of stapes and incus frequency responses under implanted condition are reduced below 1 kHz. However, this variation does not exceed the limits of the standard deviation response of the stapes and incus frequency responses of healthy human middle ears.*

Keywords: *Cochlear Implant, Middle Ear, Flat Flexible Cable, Finite Element Method*

1. INTRODUCTION

The human auditory system allows the perception of sound through complex mechanisms of transduction and processing, ultimately ensuring communication by sound signals. Pathological conditions can cause hearing loss, that can be classified into conductive hearing loss or sensorineural loss. Those affected with hearing loss face barriers in educational development, socialization, and economic productivity (Tefili *et al.* (2013)). For cases of severe to profound loss, the cochlear implants (CI) is one of the possible treatments. Also for sensorineural hearing loss, CI's are not only the most successful alternative in the recovery of sensory deprivation, but often the only option (Krogmann and Khalili (2020)). Traditionally, the CI has two parts, an external and an internal one. The external one consists of microphone(s), processor, and antenna and is attached to the head, usually behind the pina. The internal part features a receiving antenna, a processor and a current source, all of them implanted under the skin of the temporal bone, and an electrode array implanted in the vestibular scale of the cochlea. Although this technology makes it possible for the user to restore part of the hearing capabilities, the external part of the device presents several drawbacks for its users: (1) risk of the external module suffering impacts and contact with humidity (2) magnetic resonance imaging incompatibility, (3) aesthetic concerns. To avoid these problems associated with the external part of the CI, it is proposed to replace the external part with fully implantable components, allowing a better quality of life. The Laboratory of Vibrations and Acoustics at UFSC (LVA) focuses on the development of a Totally implantable cochlear implant (TICI) prototype. The works developed at LVA (Gesing *et al.* (2016, 2017); Calero *et al.* (2018); Gesing *et al.* (2018, 2019)) presented alternatives for capturing the sound field without the need for an external microphone by means of a vibration sensor manufactured with MEMS technology (Micro-Electro-Mechanical System) that can be implanted in the human middle ear (ME). This sensor captures the sound event in terms of the acceleration of the incus, one of the osscicles of the ossicular chain.

In addition to a sensor for a TICI, a cable responsible for the connection between sensor and electronic components must be developed in such a way as to minimize its influence on the dynamic response of the ossicular chain. While several proposals for implantable sensors are described in the literature (Calero *et al.* (2018)), only very few reports on the development of suitable electrical connections are available. In fact only two references were identified by the authors: In Park *et al.* (2007) a proposal for a flat flexible cable (FFC) is presented, and experimental data on the behaviour of such a cable when implanted in cadaveric human middle ears is reported. Another FFC to operate with a vibration sensor in the ME is described in Soydan (2019). Soydan present a feasible and 3D integration between sensor, energy harvester and cable for applications that required low weight, flexible and robust integration but does not look into the impacts on ME vibration.

The scope of the present work is to analyze the dynamics of the FFC presented in the literature and secondly to propose an authorial FFC and to evaluate its influence on the human ME dynamics.

2. METHOD

In this section, FFC designs described in the literature are presented. Analytical and numerical modal analyses are preformed to evaluate their dynamic behavior. Using the finite element method (FEM) models of the cables, their mechanical lumped parameters are obtained for performing a preliminary analysis of their influence on the OM. Finally, based on a the FFC described in the literature, a cable was developed to be fitted to the sensor developed at LVA and its effects on the ME dynamics are studied via a complete FE model of the cable, the sensor attached to the incus by means of a clamp and the middle ear itself.

2.1 FFC described in the literature

The FFC proposed in Park *et al.* (2007), labeled to as cable 1 in this work, uses a sandwich structure with copper traces between two layers of polyimide (PI) for insulation as seen in Figure 1. The thickness of each layer is 13 μm, while the cable's width and length are 0.525 mm and 34 mm, respectively. All three traces are 75 μm wide and also spaced 75 μm apart.

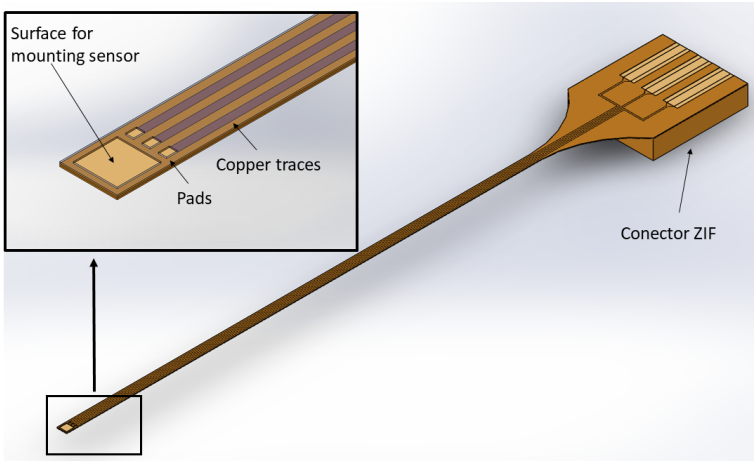

Figure 1: 3D drawing of cable 1 with the details of the location to connect the sensor.

The second proposal, named cable 2 herein, was developed in Soydan (2019). Its structure is similar to that of cable 1. It features a 35 μm thick parylene C layer and 0.5 μm thick gold traces that are coated with another 1 μm layer of parylene C. Figure 2 shows the design of cable 2 with its dimensions: 3.4 mm width, 35 mm length, and 36 μm thickness.

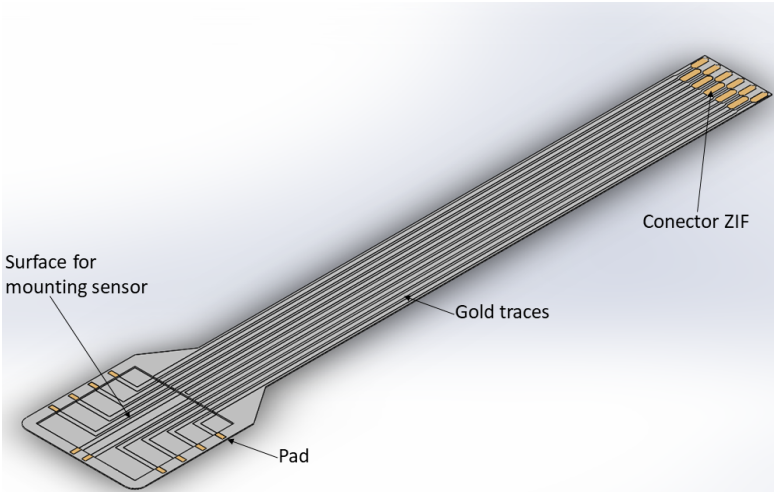

Figure 2: 3D drawing of cable 2.

FEM models of both cables were built using the Solid Mechanics module of COMSOL Multiphysics 5.2. Material properties for PI and copper were taken from the MEMS material library program, while the data for parylene-C were extracted from the literature (Teo *et al.* (2016); Soydan (2019); VSiParylene (2020)). All properties are given in Table 1.

Geometrically both cables are cantilevered cables as shown in the Figure 3. For cable 2 the gold layer was neglected in the FE model because if its thickness of only 0.5 μm. Both cables were considered in the fixed-free boundary conditions,

Table 1: Properties of the materials used in the FCC.

Material	Property	Symbol	Value
PI	Density	ρ	1300 kg/m^3
	Young Modulus	E	3,1 GPa
	Poisson	ν	0,34
Parylene C	Density	ρ	1289 kg/m^3
	Young Modulus	E	2,8 GPa
	Poisson	ν	0,34
Copper	Density	ρ	8960 kg/m^3
	Young Modulus	E	120 GPa
	Poisson	ν	0,34

because one end of the cables is embedded in the temporal bone while the other is freely vibrating. Therefore, only 10 mm of the cable's length, corresponding to the part between sensor and ME cavity wall, was considered free to vibrate. The length of the free part was estimated from a 3D model of the temporal bone, by taking the distance between the incus, the ossicle where the sensor is placed, and the end of the ME access channel, as seen in Figure 4.

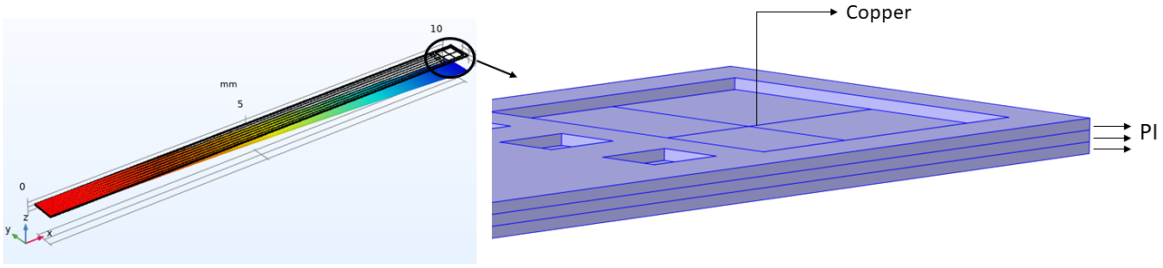

Figure 3: Free end of Cable 1 in cantilever condition and close-up of the sensor positioning pad.

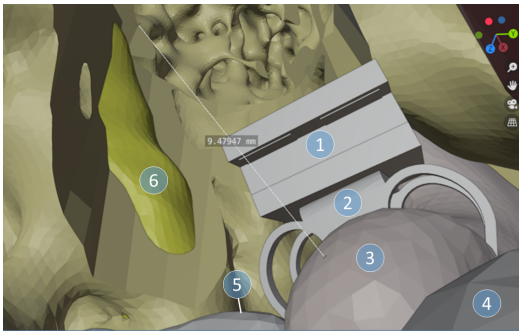

Figure 4: 3D model of the human ME cavity with the implated sensor (1), clip (2), incus (3) , malleus (4), stapes (5) and facial nerve (6).

Mesh sizes used for cables 1 and 2 were defined based on the wavelength propagating in a beam and plate respectively and defined as

$$\lambda_{\text{beam}} = 2\pi \left(\frac{EI}{\omega_{\text{max}}^2 m_{\text{b}}} \right)^{1/4} \tag{1}$$

and

$$\lambda_{\text{plate}} = 2\pi \left(\frac{Eh^3}{12(1-\nu^2)\omega_{\text{max}}^2 m_{\text{p}}} \right)^{1/4} \tag{2}$$

wherein $\omega_{\text{max}} = 2\pi f_{\text{max}}$ is the maximum angular frequency of the analysis, $f_{\text{max}} = 20$ kHz (upper limit of human hearing)), m_{b} is the mass per unit of length, m_{p} is the mass per unit of area, E is the Young's modulus and I the moment of inertia of the beam. To guarantee the accuracy of the numerical computation, the element size is about 1/17 of the wavelength. Cable 1 is therefore composed of 3,667 tetrahedral elements, while cable 2 used 39,824 tetrahedral elements.

2.2 Simplified analysis of the effects of cable 1 and 2 on the middle ear dynamics

The influence of cable 1 and 2 on the human ME was carried out using a FE model of the human ME developed by Lobato (2019) and representing the cables by a lumped element system coupled to this ME FE model. Two FRFs were obtained in the analyses: The mobility response of the stapes footplate (H_{fp}), since this FRF is widely discussed in the literature and its function is to validate the present ME model; and the incus mobility FRF (H_{incus}), aiming to assess whether the incus maintains its natural dynamic behavior, as the TICI input signal to be captured by the implanted sensor results from its movement.

The FE model of the human ME consists of the tympanic membrane, ossicular chain, ligaments, and tendons, all obtained by microtomography. Only the superior ligament of the malleus was not generated by microtomography but approximated by a cylinder as shown in Figure 5. The ME models mesh has 38,825 tetrahedral elements and the constitutive model of the structures was defined as linear elastic with the properties discussed in Lobato (2019).

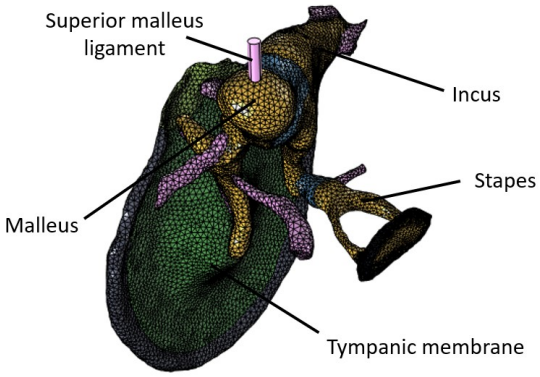

Figure 5: FE model of the human middle ear.

To consider the effects of the cable's implantation, the cables were incorporated into the ME model via a lumped parameter model applied to one face of an element of the incus' long process, as shown in Figure 6.

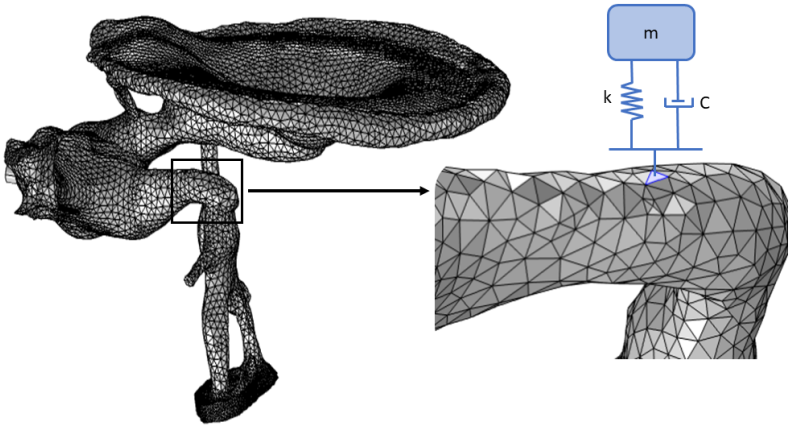

Figure 6: Lumped parameter model of the cable attached to one face of an element of the incus' long process in the human ME FE model.

The added inertia consists of the equivalent mass at the end of the cables. The equivalent stiffness was estimated through static analysis wherein the cable section clamped in the ME cavity wall was subjected to a unit force (1 μN) applied on the sensor positioning pad to reproduce tensile and flexion load cases as shown in Figure 7. The ratio between pad displacement and force represents in this case the equivalent flexural stiffness of the cables. The damping property of the cables was simplified by structural damping of PI obtained from Benabed (2014) and shown in Table 2.

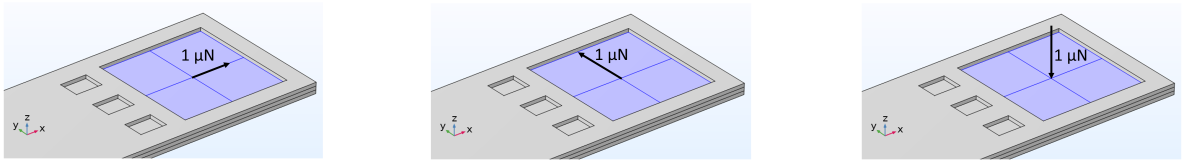

(a) tensile case (x-axis). (b) lateral bending case (y-axis). (c) transversal bending case (z-axis).

Figure 7: Static loads applied to obtain cables stiffness.

Table 2: Lumped mechanical parameters of cables 1 and 2.

Cable	Stiffness (N/m)			Mass (mg)	Structural damping - η
	k_{xx}	k_{yy}	k_{zz}		
1	18,400	21	0.45	0.5	0.001
2	3,831	2,034	0.35	2.4	0.001

2.3 Analysis of the effects of proposed cable on middle ear dynamics

Based on cables 1 and 2, an authorial cable was proposed in this work. The analysis of its influence on the human ME dynamics was realized incorporating its FE model into the FE model of the human ME. To consider its real application condition, other components of the TICI were also inserted in the FE model, namely the clamp and the sensor.

The proposed cable (Figure 8) was designed incorporating features from both cables 1 and 2. The width of the authorial cable was defined to be 0.5 mm because, in addition to allowing greater lateral flexibility, it allows the surgeon to better visualize the access to the middle ear. Conductive traces were designed to be similar to those of cable 2, since they are much thinner than the traces of cable 1 and become negligible in transverse bending, which reduces the influence of stiffness added to ME. The sensor positioning region was resized to enable the fixation of the sensor developed by our lab and described in Cartagena Miron (2022). The other extremity to be connected to the electronics of the TICI kept the dimensions of cable 1, and a smooth transition with a radius of 5 mm is adopted to avoid stress concentration.

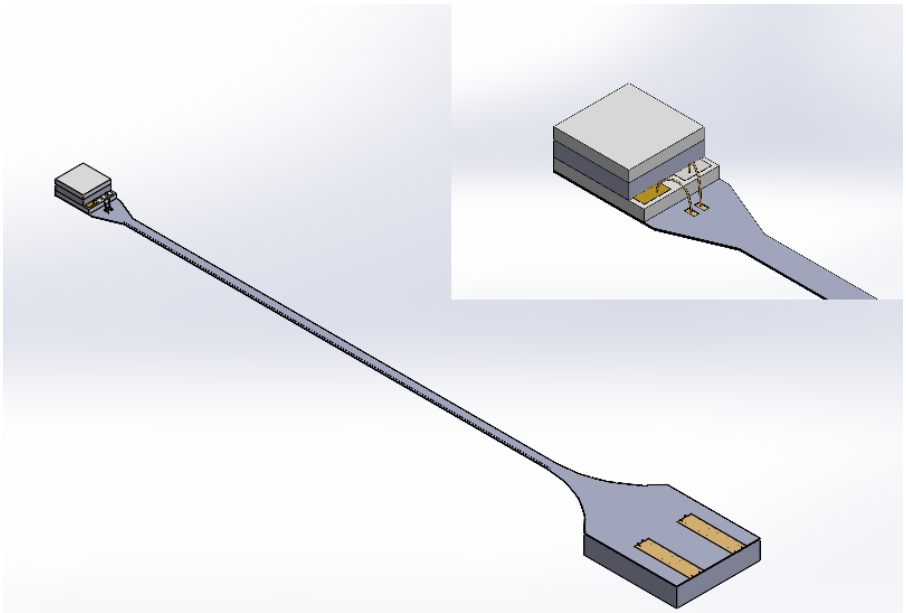

Figure 8: Cable proposed, fitted with the vibration sensor.

To add the clamp to the ME model, a quasi-static analysis was performed using the Solid Mechanics module in COMSOL. The clamp was positioned close to the long process of the incus and then a sequence of stationary studies with steps of clamps displacements was imposed until reaching the fitting position. The mesh generated for each study is automatically refined by the software so that the results converge. The stress and final mesh is shown in Figure 9.

Once the clamp's mesh fixed to the incus' long process is obtained, it is placed in the FE model of the ME. The geometries of the proposed cable and sensor are also incorporated into the FE model. The adopted boundary conditions

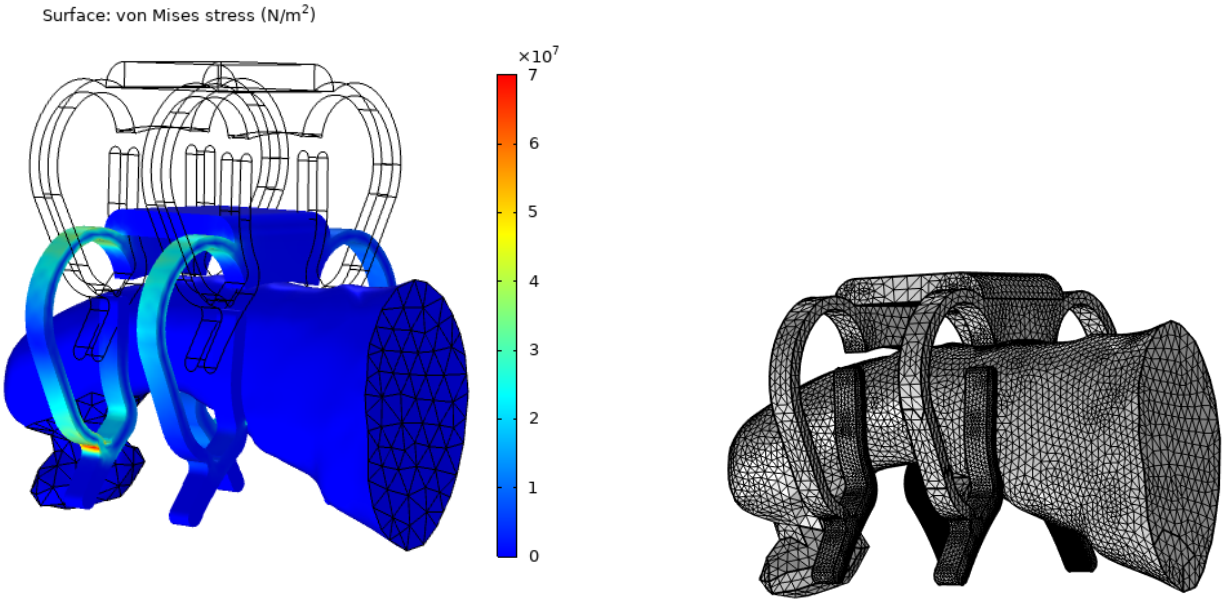

Figure 9: Positioning and meshing of the clamp at the long process of the incus.

considered two simplifications: (1) displacements of the incus and clamp are equal in the contact region and (2) the section of the cable embedded in the ME cavitity wall is fixed, as shown Figure 10.

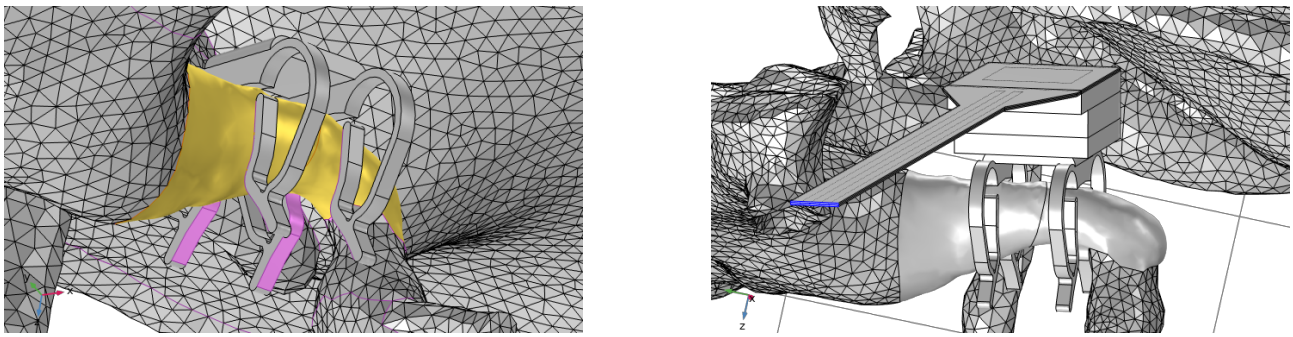

(a) Rigid contact between clamp and incus' long process.

(b) Section of the cable clamped.

Figure 10: Boundary conditions in the complete FE model.

3. RESULTS

3.1 Modal analysis

For understanding the dynamic behavior and to validate the FE models, a modal analysis in fixed-free conditions was carried out, because there is a closed analytical solution for comparison. Figure 11 shows three vibration modes for cable 1 obtained using the FE model descibed above. Up to 10 kHz, nine mode shapes (bending and torsion modes), with a predominance of bending modes in the transverse direction, were identified. As the cable does not present a natural frequency close to 1000 Hz, there is no overlap with the resonance frequency of the human middle ear (Lobato *et al.* (2022)). The numerical model resulted in natural frequencies very close to the analytical solution for a cantilevered beam, as shown in Table 3. It can also be seen that for lateral bending modes, the traces must be considered, as these increase the bending stiffness of the cross-section, hence their absence implies in an absolute error of 32%. For the geometry of cable 1, it is concluded that the Euler-Bernoulli theory is applicable to predict the cable's natural frequencies.

Cable 2 presented 19 vibration modes up to 10 kHz, including transverse bending and torsion. The first two modes are similar to those for a beam in bending and torsion as shown in Figure 12. However, other modal forms are the transverse deflections that depend on their lateral directions (x and y), which characterizes the mechanical response of a plate. For comparison, as seen in Table 4, the natural frequency solutions of a uniform beam, a two-section beam, and a rectangular plate were evaluated. However, no analytical model showed good agreement for all calculated modes.

The modal analysis of the cable proposed by the authors of this work (Figure 8) showed 10 modes up to 10 kHz, including transverse bending, lateral bending and torsion modes. Figure 13 presents the first three modal shapes, which

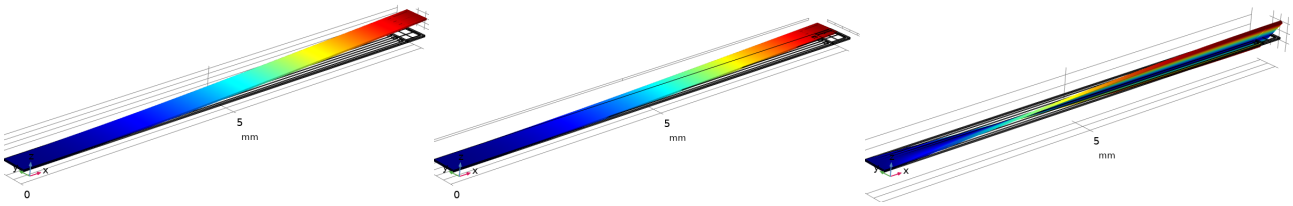

Figure 11: The firsts bending and torsion mode shapes of cable 1 obtained by FE analysis.

Table 3: Comparison between the natural frequencies of cable 1 obtained by analytical models and the cable's FE-model.

Mode	Type	FE-model (Hz)	analytical model (Hz)	absolute error (%)	analytical model (Hz)	absolute error (%)
1	Bending z	96	97	1.04	91	5.87
2	Bending z	570	609	6.80	568	0.46
3	Bending z	1595	1707	7	1590	0.33
4	Bending y	2058	1396	32	2076	0.86
5	Bending z	3130	3347	6.90	3119	0.44
6	Torsion	3523	3538	0.20	-	-
7	Bending z	5180	5817	12.30	5420	4.60
8	Bending$z$	7753	8473	9.20	7894	1.80
9	Torsion	10575	10613	0.36	-	-

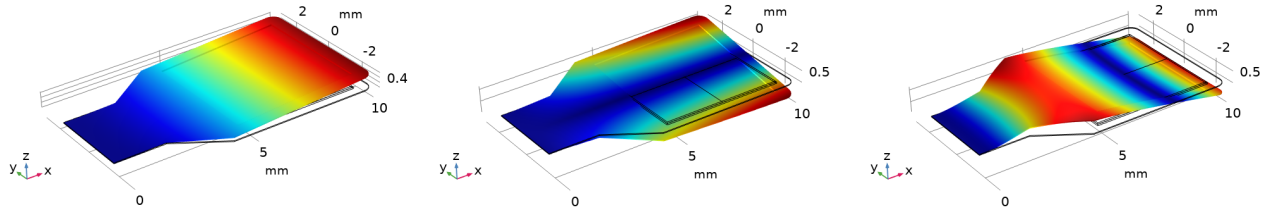

Figure 12: First three mode shapes for cable 2 obtained by FE analysis.

Table 4: Comparison between natural frequencies of cable 2 using different analytical models for a simple beam, a stepped beam and a plate and the FE-model of cable 2.

Mode	Type	FE-model	analytical beam model (Hz)	absolute error (%)	analytical stepped beam model (Hz)	absolute error (%)	analytical plate model (Hz)	absolute error (%)
1	Bending z	68	83	22	63	7	87	28
2	Torsion	263	263	0,2	-	-	375	41
3	Bending z	624	522	16	499	20	542	13
4	Torsion	1051	791	25	-	-	1247	19
5	Bending z	2176	1462	33	1467	33	1437	34
6	Bending z	2856	2868	0.4	2858	0.01	2115	26

are similar to those of cable 1. As verified in Table 5, the proposed cable exhibits natural frequencies that are very close to the ones obtained using an analytical beam model. It is also noted that for the fourth mode the traces have a great influence on lateral flexion.

3.2 Dynamic response of the human ME with cable 1 or 2 attached

To evaluate the dynamic response of the human ME with cable 1 or 2 attached, the mobility FRF of the stapes and incus was computed using the FE model described in Section 2.2which features lumped parameter representations of the cables.

Figure 14 presents the magnitude of the mobility FRFs of the stapes and incus. The curve in black was obtained experimentally (Aibara *et al.* (2001)), the blue curve is generated by the FE model from the ME only and the curves in green and red are from the same ME FE model but incorporating the lumped parameter representation of cables 1 and 2 respectively.

It is noted that the two cables have similar effects, as the mobility functions overlap in almost the entire spectrum. The cables introduce a small stiffness increase into the system, which can be seen by the shift of the FRFs peak from 1000

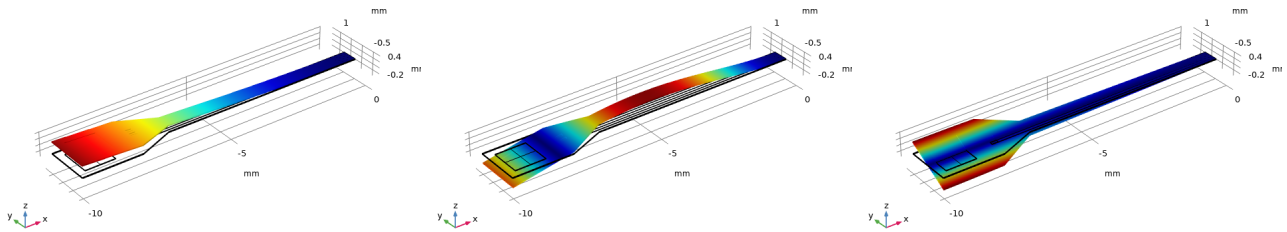

Figure 13: The firsts three mode shapes of proposed cable.

Table 5: Comparison between the natural frequencies of the proposed obtained by analytical models and the cable's FE-model.

Mode	Type	FE-model (Hz)	analytical beam model (Hz)	absolute error (%)	analytical stepped beam model (Hz)	absolute error (%)
1	Bending z	63	60	5	73	16
2	Bending z	514	538	5	503	2
3	Torsion	1138	-	-	-	-
4	Bending y	1215	775	36	1100	0.86
5	Bending z	1543	1631	6	1520	0.44
6	Bending z	3137	3408	9	3184	1.5

Hz to 1250 Hz. Although cables 1 and 2 have very different widths and masses and, consequently, lateral stiffnesses and inertias, the incus response considering the cables becomes different only above 8 kHz, where the incus' response with cable 2 attached decreases. It can be concluded that in the entire frequency range relevant for speech (110 -6 kHz) the cables' presence only shifts the peak from 1 kHz to 1.25 kHz for this particular ME.

3.3 Finite element model of the human ME including the proposed cable

The first analysis of the proposed cable's effect on the dynamics of the ME verified the change in the natural frequencies of the ME, attaching the clamp only; the clamp and the sensor; and the clamp, sensor and cable. As can be seen in Table 6, the insertion of the clamp with a mass of approximately 1.5 mg and the sensor with amass of 3.8 mg have very little influence on the dynamics of the middle ear, with the greatest variation being 3.75% for the third natural frequency. The cable has greater influence on two first modes, shifting their natural frequencies due to stiffness added to the system. The maximum change was almost 11%, which is a moderate change indicating that the proposed design is promising for its application.

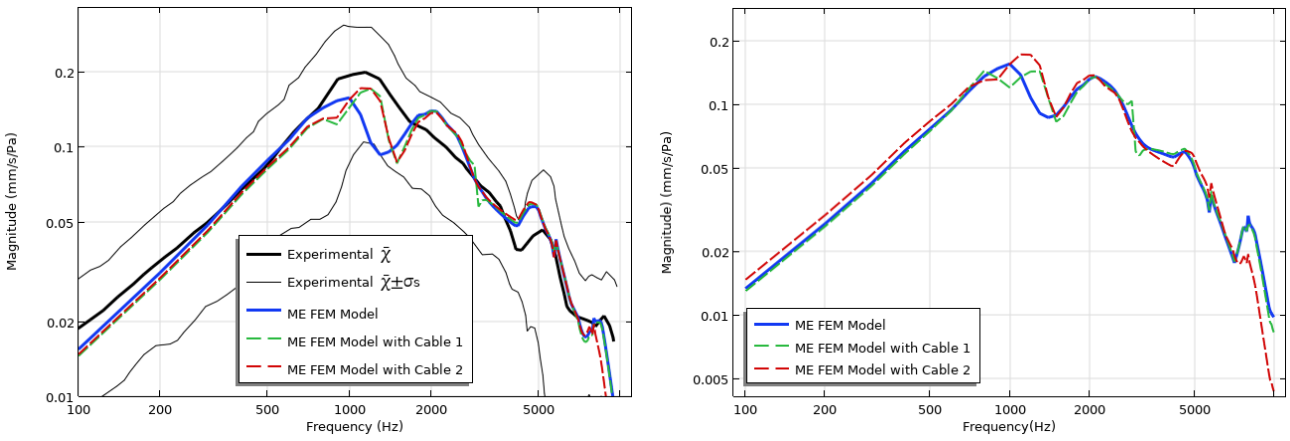

(a) Stapes mobility FRF.

(b) Incus mobility FRF.

Figure 14: Human ME's stapes and incus magnitude FRFs. Black curve shows experimental data Aibara *et al.* (2001), blue curve obtained by the FE model of the ME alone, green and red curves for the same ME model but incorporating the lumped parameters of cables 1 and 2.

Table 6: Comparison of human ME natural frequencies with TICI components attached.

ME only	ME with clamp		ME with clamp and sensor		ME with clamp, sensor and cable	
Natural frequency	Natural frequency	Δ (%)	Natural frequency	Δ (%)	Natural frequency	Δ(%)
1,128 Hz	1,141 Hz	1.2	1,121 Hz	-0.6	1,210	7.3
1,165 Hz	1,194 Hz	2.5	1,183 Hz	1.5	1,288 Hz	10.6
1,920 Hz	1,919 Hz	-0.05	1,992 Hz	3.75	1,992 Hz	3.75
2,071 Hz	2,070 Hz	-0.05	2,066 Hz	-0.2	2,034 Hz	-1.8

The second study corresponds to the harmonic analysis, which used the direct method to obtain the stapes and incus mobility functions at frequencies from 100 Hz to 10 kHz. The frequency response curves shown in Figure 15 confirm the results of the modal analysis. The clamp and the sensor (red curves) do little to change the ME response and the cable is the component with the largest influence on the middle ear dynamics. The stiffness causes the reduction of the FRF's magnitude in low and medium frequencies and the shift of the first two peaks to higher frequencies.

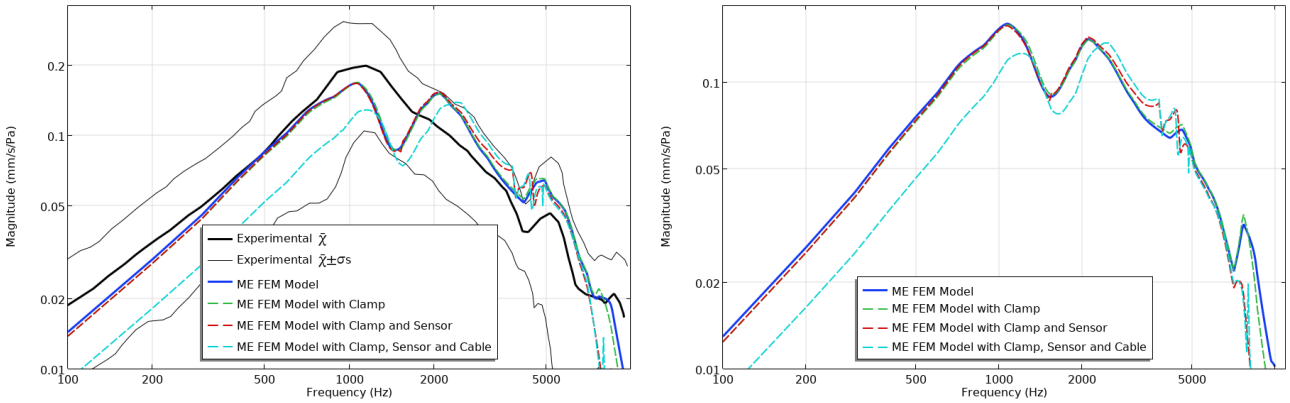

(a) Stapes mobility.

(b) Incus mobility.

Figure 15: Magnitude of the stapes and incus FRFs. Black curve shows experimental data, blue curve is for the ME only, green, red, and cyan curves for the same ME model, but gradually incorporating clamp, sensor, and cable.

4. CONCLUSION

A flat flexible cable (FFC) proposed for the use as a part of a totally implantable cochlear implant was analyzed in terms of its influence on the ME dynamics. The cable was developed based on two other designs described in the literature, using conductive traces on layers of flexible polymers. The frequencies and modal shapes determined using an FE model of one of the reference cables (cable 1) are very close to the frequencies and modal shapes determined by analytical models using the Euler-Bernoulli beam theory. The other reference cable presented a different vibration behavior, with its vibration modes dependent on the two lateral directions. Also no classic analytical model was found to represent its vibratory behavior. The numerical study on the influence of these cables on the middle ear dynamics indicated that cable 1 causes less alteration of the incus response. A FE model of the proposed cable was constructed and added to a complete FE model of the human ME. It is also seen that the addition of the cable incresed the overall stiffness of the system, shifting the FRF magnitude curve by around 200 Hz to higher frequencies. While its effect is noticeable, the proposed cable did not reduced the response at lower levels under the inferior bound of standard deviation of statistical experimental frequency response. Thus, a prominent alternative for the electrical connection of the fully implantable cochlear implant was presented.

5. ACKNOWLEDGMENTS

The authors would especially like to thank Lucas Costa Lobato for supporting this work by providing the finite element model of the human middle ear and for giving suggestions during the revision of this manuscript.

6. REFERENCES

Aibara, R., Welsh, J.T., Puria, S. and Goode, R.L., 2001. "Human middle-ear sound transfer function and cochlear input impedance". *Hearing Research*, Vol. 152, pp. 100–109.

Calero, D., Paul, S., Gesing, A., Alves, F. and Cordioli, J.A., 2018. "A technical review and evaluation of implantable sensors for hearing devices". *BioMedical Engineering OnLine*, Vol. 17, p. 23.

Gesing, A.L., Arellano, D.C., Murta, B., Paul, S. and Cordioli, J.A., 2016. "A study on the feasibility of a mems piezoelectric accelerometer coupled to the middle ear as sensor for totally implantable hearing devices". In *Proceedings of the 22nd International Congress on Acoustics*. Buenos Aires, Argentina.

Gesing, A.L., Masson, Z.N., Arellano, D.C., Alves, F., Paul, S. and Cordioli, J.A., 2019. "Middle ear ossicular chain vibration detection by means of an optimized mems piezoelectric accelerometer". *IEEE Sensors Journal*, Vol. 19, pp. 2079–2086.

Gesing, A.L., Murta, B., Kohler, L.O., Junckes, M., Weirich, R., Paul, S. and Cordioli, J.A., 2017. "Caracterização numérica e experimental de acelerômetro piezoelétrico com circuito de pré-amplificação". In *Anais do Encontro da Sociedade Brasileira de Acústica*. Brasília, Brasil.

Gesing, L.A., Alves, F.D.P., Paul, S. and Cordioli, J.A., 2018. "On the design of a MEMS piezoelectric accelerometer coupled to the middle ear as an implantable sensor for hearing devices". *Scientific Reports*, Vol. 8, p. 3920.

Krogmann, R.J. and Khalili, Y.A., 2020. "Cochlear implants". In *StatPearls*, StatPearls Publishing, Treasure Island (FL).

Lobato, L.C., 2019. "How stapes ankylosis and fracture affect middle ear dynamics: A numerical study". *Journal of Biomechanical Engineering*, Vol. 141, p. 111011.

Lobato, L.C., Paul, S. and Cordioli, J.A., 2022. "Statistical analysis of the human middle ear mechanical properties". *The Journal of the Acoustical Society of America*, Vol. 151, pp. 2043–2054.

Park, W.T., O'Connor, K.N., Chen, K.L., Mallon, J.R., Maetani, T., Dalal, P., Candler, R.N., Vitikkate, V.A., Roberson, J.B., Puria, S. and Kenny, T.W., 2007. "Ultraminiature encapsulated accelerometers as a fully implantable sensor for implantable hearing aids". *Biomedical Microdevices*, Vol. 9, pp. 939–949.

Soydan, A.K., 2019. *System integration of MEMS devices on flexible substrate for fully implantable cochlear implant applications*. Master's thesis, Middle East Technical University.

Tefili, D., Barrault, G.F., Ferreira, A.A., Cordioli, J.A. and Lettnin, D.V., 2013. "Implantes cocleares: aspectos tecnológicos e papel socioeconômico". *Rev. Bras. Eng. Bioméd., vol.29, n4, p.414-433, 2013*.

Teo, A.T., Mishra, A., Park, I., Kim, Y.J., Park, W.T. and Yoon, Y.J., 2016. "Polymeric Biomaterials for Medical Implants and Devices". *ACS Biomaterials Science & Engineering*, Vol. 2, pp. 454–472.

VSiParylene, 2020. "Parylene properties". , https://vsiparylene.com/parylene-properties/. Accessed 12 Aug 2023.

7. RESPONSIBILITY NOTICE

The authors are solely responsible for the printed material included in this paper.